AIP | Journal of Applied Physics

Focused-ion-beam overlay-patterning of three-dimensional diamond structures for advanced single-photon properties

Qianqing Jiang, Dongqi Liu, Gangqin Liu, Yanchun Chang, Wuxia Li, Xinyu Pan, and Changzhi Gu

Citation: Journal of Applied Physics **116**, 044308 (2014); doi: 10.1063/1.4891022
View online: http://dx.doi.org/10.1063/1.4891022
View Table of Contents: http://scitation.aip.org/content/aip/journal/jap/116/4?ver=pdfcov
Published by the AIP Publishing

JOURNAL OF APPLIED PHYSICS **116**, 044308 (2014)

Focused-ion-beam overlay-patterning of three-dimensional diamond structures for advanced single-photon properties

Qianqing Jiang,[1] Dongqi Liu,[1] Gangqin Liu,[1] Yanchun Chang,[1] Wuxia Li,[1,a)] Xinyu Pan,[1,2] and Changzhi Gu[1,2,a)]
[1]*Beijing National Laboratory of Condensed Matter Physics, Institute of Physics, Chinese Academy of Sciences, Beijing 100190, China*
[2]*Collaborative Innovation Center of Quantum Matter, Beijing 100190, China*

(Received 25 March 2014; accepted 4 July 2014; published online 25 July 2014)

Sources of single photons are of fundamental importance in many applications as to provide quantum states for quantum communication and quantum information processing. Color centers in diamond are prominent candidates to generate and manipulate quantum states of light, even at room temperature. However, the efficiency of photon collection of the color centers in bulk diamond is greatly reduced by refraction at the diamond/air interface. To address this issue, diamond structuring has been investigated by various methods. Among them, focused-ion-beam (FIB) direct patterning has been recognized as the most favorable technique. But it has been noted that diamond tends to present significant challenges in FIB milling, e.g., the susceptibility of forming charging related artifacts and topographical features. In this work, periodically-positioned-rings and overlay patterning with stagger-superimposed-rings were proposed to alleviate some problems encountered in FIB milling of diamond, for improved surface morphology and shape control. Cross-scale network and uniform nanostructure arrays have been achieved in single crystalline diamond substrates. High quality diamond solid immersion lens and nanopillars were sculptured with a nitrogen-vacancy center buried at the desired position. Compared with the film counterpart, an enhancement of about ten folds in single photon collection efficiency was achieved with greatly improved signal to noise ratio. All these results indicate that FIB milling through overlay patterning could be an effective approach to fabricate diamond structures, potentially for quantum information studies. [http://dx.doi.org/10.1063/1.4891022]

I. INTRODUCTION

Diamond is an important material for its outstanding properties in many aspects.[1–3] In recent years, increasing attentions have been drawn on this shinning material for its very promising prospect in quantum information processing, benefit from the abundant color centers which naturally exist in or been artificially introduced into the material, of particular interest is the nitrogen-vacancy (NV^-) centers.[4–14] The electron spin of NV^- centers in diamond can be initialized, coherently controlled, and read out at room temperature.[7] The robust spin coherence[9] and optical addressability via spin-dependent orbital transitions[10] offer such systems with great potential in applications ranging from quantum information processing[11–14] to nanoscale electric field sensing.[4,15,16] Therefore, NV^- centers have been considered as one of the most important individually addressable qubit systems. However, in bulk diamond crystals, it has the disadvantage of low photon out-coupling. In that, investigations, to improve the in- and out-coupling of photons, have been conducted to manipulate the light–matter interactions by embedding the NV^- centre within diamond photonic structures.[17–19] Compared with the bulk diamond crystal, the merits of the freestanding diamond micro-/nanostructure with NV^- center embedded are many folds, including: (i) the optical power coupling from a pump laser to an NV^- centre embedded structure allows for an order of magnitude more efficient excitation; (ii) the nanostructures could modify the far-field emission of the NV^- centers, as a consequent, it facilitates the collection of emitted photons; (iii) the fluorescence lifetime of an NV^- centre in the structured diamond can be increased due to the reduction of the background refractive index ($n \approx 2.4$ for the bulk and $n \approx 1$ for nanoparticles). Thus, structured diamond single photon source could have much enhanced photon collection efficiency with much higher magnitude of single-photon flux.[20]

Therefore, micro-/nanofabrication are essential to fully realize the potentials of diamond in the recently blooming research fields. Up to now, various top-down nanofabrication techniques have been explored for well-designed diamond structures.[17–20] One of these approaches is to evanescently couple a separate optical cavity or a waveguide to a proximal NV^- center.[21] Another approach is to realize optical structures, e.g., vertically oriented nanowire antennas in a single-crystal diamond substrate, to mechanically isolate individual NV^- centers and minimizes background fluorescence.[20] Focused-ion-beam (FIB) methods are attractive for machining at the micro-/nanoscale, since almost any solids, including hard materials, can be shaped by ion beams. Recently, it has been demonstrated that FIB is suitable for diamond optical prototype processing due to its great design-ability, controllability, and flexibility.[22] The beneficial of FIB processing also includes the negligible force and heat

[a)]Authors to whom correspondence should be addressed. Electronic addresses: liwuxia@aphy.iphy.ac.cn and czgu@aphy.iphy.ac.cn

imposed on a target, excellent beam positioning accuracy, large depth of focus, and stable operating conditions. However, for structures with curved surfaces, especially for single photon source structures that require good couture and smooth surface, it is still a big challenge and advanced approaches are highly demanded.[23]

In this work, we took the FIB system as the fabrication tool to produce various diamond 3D structures, especially with NV^- centers embedded precisely at the designed position within the structure for improved properties as a single photon source. We first investigated the effects of crystallographic properties, ion stray dose, and charging on patterning of diamond. Then, advantageously, based on these effects, stagger-superimposed-rings were used for high quality curved surface structure fabrication. Furthermore, we developed a simple but effective strategy, periodically-positioned-rings patterns to fabricate cross-scale and hierarchy structure arrays, which were found to have very smooth surface and well-controlled size, shape, and distribution. As typical examples, diamond solid immersion lens (SILs) and pillars with single NV^- centre embedded were composed for single photon properties characterizations. Single photons count rate measurement indicates an enhancement of about ten folds in the photon collection efficiency compared with the un-sculptured diamond crystal. The $g^{(2)}(\tau)$ and Ramsey fringes measurements showed that the FIB processing did not affect the single photon emission and the coherent properties. Our results suggest that the presented method may enable a new approach for fabrication of high quality quantum devices based on structured diamond, including serving as sensors to detect the various field parameters in 3D distributed spots simultaneously with nanometer scale accuracy.[4,24]

II. EXPERIMENTAL METHOD

Direct construction of diamond 3D nanostructures was carried out using an FEI dual beam FIB/SEM system. The used ion (liquid gallium) beam energy was 30 keV and the ion beam currents were in the range of 1.1 pA–69 nA. *In-situ* SEM imaging was conducted to monitor the shape and geometry evaluation of the resulted structures. Two methods were employed to remove the FIB processing induced contamination completely. The first method was by reactive ion etching in a gas mixture of O_2 and CHF_3 (O_2: CHF_3 = 30:4 sccm), the chamber pressure was 10 mTorr for 20 min. The incident power was 100 W and the DC bias was 340 V. The fabricated solid immersion lens was treated using the first method. The other approach was using inductive coupled plasma etching (ICP) followed by wet etching. The ICP processing time is 1 min, the used reactive gas was a mixture of O_2 and Ar (O_2:Ar = 50:50 sccm), the ICP power and reactive ion etching (RIE) power for processing were 500 W and 200 W, respectively. For the wet etching, a mixture of HNO_3:H_2SO_4:$HClO_4$ = 1:1:1 (volume) was used with the sample immersed in the solution for 18 h, which was heated to 208 °C in oil. The sample was then transferred to a bath of HF aqueous solution (40% in volume), which was maintained at 60 °C for 12 h. The second treatment was conducted on the FIB processed nanopillars and network structures. The fluorescence scanning and the single photon count rate measurement were carried on a home-built laser scanning confocal microscope system which can detect single photon fluorescence and has sub-micrometer precision. During measurement, a 532-nm continuous wave laser beam was switched on and off by an acoustic optical modulator (AOM); an X-Y galvanometer was used to control the scanning of the laser spot before it was directed to the sample through a microscope objective. The spin state-dependent fluorescence of the NV^- centre was collected by the same objective, which was then filtered by a 532 nm notch and a 650 nm long path. After that, the weak light signal was translated into the electronic pulse signal by a single-photon counting module and was subsequently counted by a pulse counter or to a Hanbury-Brown and Twiss detection system to record the second order intensity correlation function [$(g^{(2)}(\tau)$)].

III. RESULTS AND DISCUSSION

A. Diamond patterning with conventional FIB approach

When an energetic ion impacts with a target material, a collision cascade in the target material can be produced. Surface sputtering occurs when the normal component of momentum received by a surface atom from the collision cascade exceeds its surface binding energy. There are various factors that affect the sputtering process, e.g., the atomic number, energy, and angle of incidence of the ion beam, and the atomic density, surface binding energy, and crystallographic orientation of the target. Among these factors, the relative orientation of the crystal plane to the incident ion beam as well as the conductivity of the target material is of particular importance in patterning, which could seriously affect the topography of the resulted structures.

Diamond is hard and not very electrically conductive. Polycrystalline diamond has different crystal planes so that the ion penetrating depth differs for different lattice spacing. In that, the crystallographic effect could result in variation of sputtering yield. Fig. 1(a) shows the SEM images of a polycrystalline diamond processed with the ion beam normal incident to the substrate surface; and Figs. 1(b) and 1(c) are for [100] orientated single crystalline diamond with the Ga^+ ions incident normal and with an grazing angle of 30° to the substrate surface, respectively. The different heights of the features on the stub walls in Fig. 1(a) tell that different grains underwent different etching rates, in consistent with the theory of crystallographic orientation dependent sputtering yield.[25] In the ion channeling direction, the channeled ions undergo mostly electronic energy losses as opposed to nuclear energy losses, thus are able to penetrate deeper into the crystal lattice. The deeper penetration and the lower probability of nuclear collisions near the surface extremely limit the probability of collision cascade caused by ions. Therefore, in the FIB milling of single crystalline diamond, ion channeling can be utilized to obtain 1D and 2D structures with flat trench bottom and smooth surface at the expense of sputtering rate.

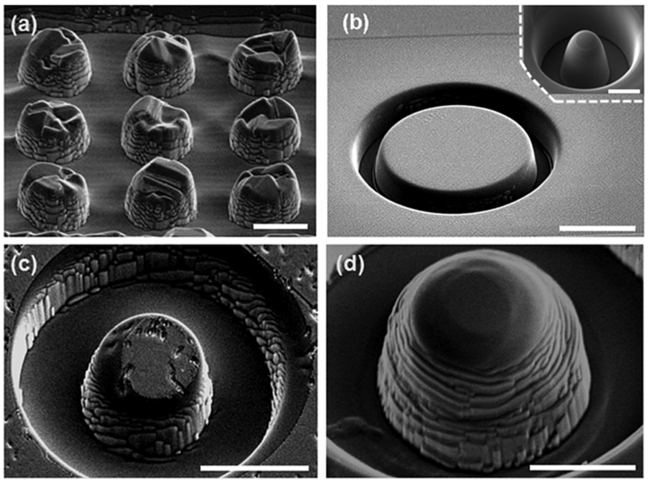

FIG. 1. SEM images showing the crystallographic orientation dependent effect on FIB construction of diamond structures: (a) stubs milled in polycrystalline diamond; (b) cylinder milled in single crystalline diamond with the ion beam incident along [100] direction, the inset shows a bell that has a higher aspect ratio; (c) cylinder milled in single crystalline diamond with ion beam incident under a grazing angle of 30° to the [100] plane; (d) hemisphere milled using folks of concentric rings that gradually decreased in inner diameter, with the ion beam incident along [100] direction. The scale bar is 5 μm and all structures were processed with ring patterns.

It is worth noticing that besides the crystallographic orientation dependent etching rate, the stray dose and charging effect are also important aspects that affect the topological properties of the milled structures. For single crystalline diamond, as shown in the inset of Fig. 1(b), the etched cylinder was clearly shrunk in the cross-sectional diameter from the bottom up to the top end, and it has ultra-smooth surface. These phenomena mainly can be attributed to the stray dose etching, charge accumulation, and transverse scattering of ions when the Ga^+ ions impinged the diamond surface. When focused-ion-beam traced outside-in in the ring area, the edges of the top part were irradiated by the laterally coming ions many more times than those in the bottom. Due to the stray dose effect, accurate fabrication of small size structures with high aspect ratio is constrained; such a phenomenon will be explained in more details at a later stage.

However, for structures with curved surfaces, besides the aforementioned effects, the geometric contrast varies across the profile of the structure, which could further result in differential sputtering rates. Fig. 1(d) shows the SEM image of a hemisphere that was milled with ion beam incident along [100] direction and folks of concentric rings were used by gradually decreasing the inner diameter of the rings systematically to achieve smooth surface. Although great efforts were paid, obvious step features are not easy to be excluded. For single photon source devices, the structures must be well-shaped and persist smooth surface, thus a developed approach is highly demanded.

B. Patterning of diamond hemisphere with Stagger-superimposed-rings

As shown above, the ion stay dose may be used for surface smoothing with the formerly sculpted structure being modified by laterally coming ions. Bear this in mind, we developed an over-lay patterning method to trim the shape and improve the surface morphology of diamond hemisphere structures. Fig. 2(a) shows the arrangement of the stagger-superimposed-rings pattern used for single crystalline diamond hemisphere fabrication. Firstly, a ring area (in blue as shown in Fig. 2(a)) was removed to form a well shaped cylinder (upper left image in Fig. 2(b)); then a second ring (red) was slightly misaligned with it to form a crescent (light red) for surface smoothening. By rotating such crescent pattern 90° in turn (light blue, light green and then light purple), a symmetrical trimming unit pattern was formed as shown inside the orange box in Fig. 2(a). By doing this, the edge formed in the previous etching step was modified in the following step with the milled area positioned within the next exposure area. With successive reduction of the outer and inner radius of the superimposed rings unit during the fabrication process, the upper part of the cylinder was dowelled gradually and a well-shaped hemisphere SIL can be expected as shown in the lower left image of Fig. 2(b). No obvious stepwise features were observed on the surface, mainly due to the rounding effect that attributed to the laterally stroking of the edges of the rough structures by the charged particles.

C. Fabrication and characterization of diamond solid state immersion lens

Now we discuss the fabrication of SILs in a [100] single crystalline diamond substrate with NV^- centers randomly distributed. Fig. 3 is the fabrication process, which includes: (i) the alignment mark fabrication by focused-ion-beam induced chemical-vapor-deposition with $W(CO)_6$ as the gas precursor by a 30 keV gallium FIB system (FEI Helios 600i); (ii) NV^- center positioning with a confocal optical microscope; (iii) thermal evaporation of 80 nm Au layer for

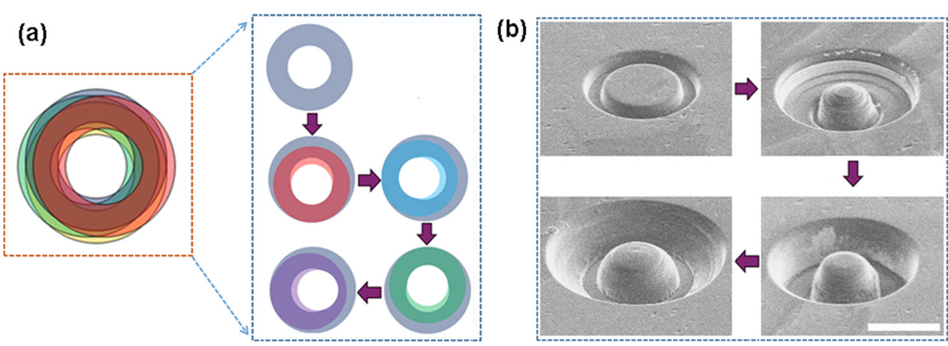

FIG. 2. Patterning of hemisphere diamond structures by stagger-superimposed-rings: (a) schematic illustration of the strategy of stagger-superimposed-rings and (b) SEM images showing the typical shape evolution of the FIB milled diamond SIL in diamond.

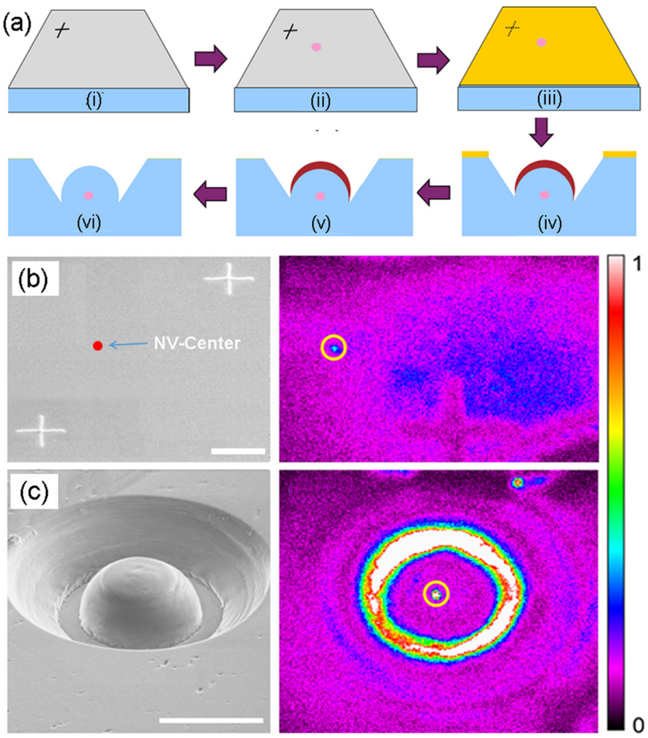

FIG. 3. (a) Work flow for the fabrication of hemisphere diamond structures by stagger-superimposed-rings: (i) Mark (black) deposition; (ii) NV^- center (pink) positioning; (iii) conducting layer (yellow) deposition; (iv) hemisphere fabrication; (v) conducting layer removal; (vi) contaminated layer (dark red) removal; (b) and (c) SEM images (left) and fluorescence scanning images (right) for the NV^- center buried in untreated diamond and the SIL center, respectively. The scale bar is 5.0 μm.

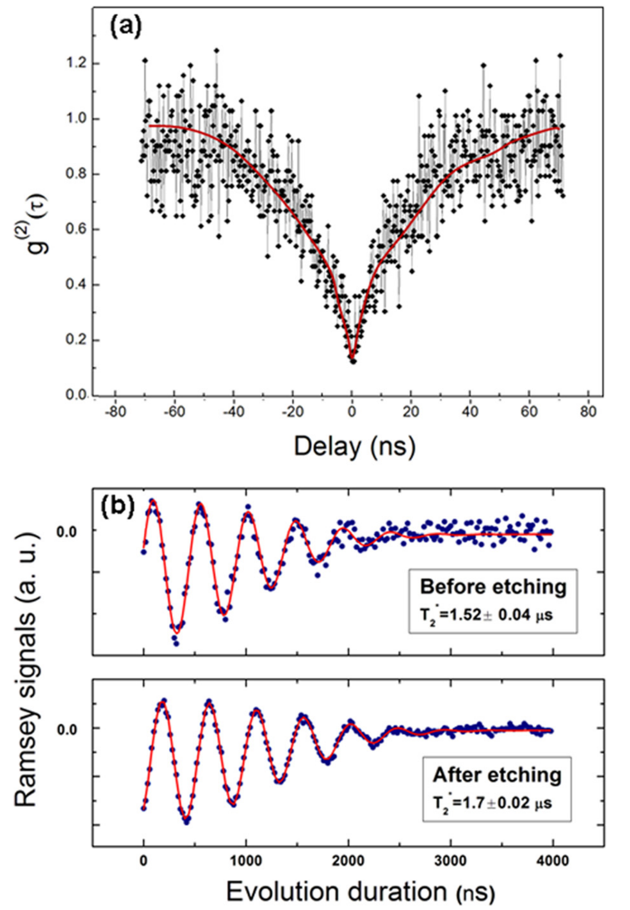

FIG. 4. Optical properties of an NV^- center embedded diamond SIL: (a) second order photon correlation function and (b) the Ramsey fringes.

charging effect suppression to assist the etching process; (iv) hemisphere construction by the aforementioned stagger-superimposed-rings patterning; (v) the conducting layer, and (vi) contamination removal by wet chemical and RIE/ICP dry etching, respectively. Thus, an NV^- center embedded SIL was fabricated as shown in Fig. 3(c).

Optical characterization was performed using a laser scanning confocal microscope system. Figs. 3(b) and 3(c) shows the SEM images and the fluorescence scanning image of the planar diamond film and the structured SIL with an NV^- center embedded, respectively. The boundary of the SIL is marked with white circle. It can be seen from the fluorescence scanning image in Fig. 3(c) that the NV^- center was very nicely placed in the center of the fabricated hemisphere. Note that the color scale has been chosen to maximize the visibility of the SIL and the surroundings—the intensity of the bright spot is about 50 kc/s and that of the structured SIL is about 480 kc/s. Single photons count rate indicates an enhancement of about ten folds in the photon collection efficiency for structure with single NV^- center buried in the SIL center (compared with the un-sculptured diamond crystal).[4,22]

The second order photon correlation function for the aimed NV^- center was also tested. Fig. 4(a) shows that the photon antibunching at delay time $\tau = 0$, the antibunching dip in the second order intensity correlation function $g^{(2)}(\tau)$, indicating clearly that the emission arises from a single center. The demonstration of strongly enhanced single photon collection efficiency from NV^- centers using SIL structures is a step toward efficient single photon sources as well as efficient optical spin read-out in compact devices. As potential building blocks for quantum repeaters,[26] cluster state computation[27] and distributed quantum computing,[28] besides the sufficient high single photon flux, the electronic spin of the NV^- centres in diamond requires excellent coherent manipulation interface. Therefore, electron-beam-lithography and thermal evaporation were used to fabricate coplanar waveguide around the structured SIL (SEM image not shown here).

Fig. 4(b) shows the free induction decay (FID) signal of the electron spin in a selected NV^- center before and after the fabrication process. The electron spin is prepared to a superposition state $1/\sqrt{2}(|m_S = 0> + |m_S = 1>)$ by a microwave $\pi/2$ pulse and is left to freely evolution under its fluctuant local field. After a delay time t, a second $\pi/2$ microwave pulse is applied to convert the accumulated phase information to population difference and readout. Thus, the dephasing time (T_2^*) can be extracted by fitting the FID signal. From these values, it can be seen that the coherent properties of NV^- electron spin were not affected by the FIB-milling process and the data points were more concentrated for the SIL, mainly due to the improved signal to noise ratio, which has increased about ten times. All the results ensure the application of the fabricated SILs in the studies of quantum science and technology.

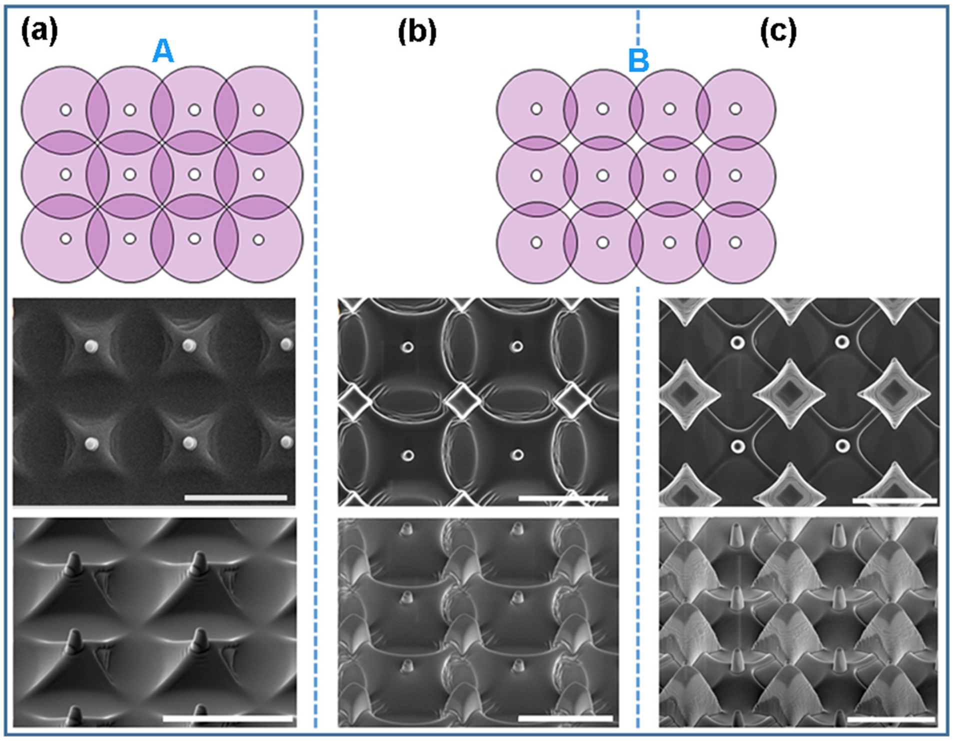

FIG. 5. FIB patterning of diamond 3D network structures with periodically-positioned-rings: the top, middle, and bottom panels are the arrangement of the ring patterns, the corresponding SEM top-view and side-view images, respectively. The ion beam current used was 2.5 nA, the inner diameter of the rings was 800 nm, and the outer diameter for patterns processed in (a) was 7 μm and those in (b) and (c) were 5 μm. The milling time for (a) and (b) was 1.25 h and that for (c) is 2.0 h. The scale bar is 5 μm.

D. Patterning of diamond network structures with periodically-positioned-rings

So far, we have demonstrated the fabrication of SIL single photon source with enhanced photon collection efficiency; however, the approach should allow an easy way to get arrays of quasi-three dimensional diamond micro/nano-structures which might raise various intriguing applications. For instance, with single NV^{-} centers buried at certain spots in the pillars of different heights, we may get a chance to measure the real 3D space distribution of temperature[23] and other physical fields. Also, quantum correlation net might be built within such complicated hierarchical structures.[29] Figs. 5(a) and 5(b) show the periodically-positioned-rings patterns used to produce hierarchical and cross-scale 3D structures. The colored rings represent the etching pattern with a denoted single ion dose, and the overlap darker areas are double-dosed, while the white areas are intact. To intuitively demonstrate the fabrication with parameters differing only in the patterns, FIB milling of single crystalline diamond was performed with patterns denoted as A and B as shown in Fig. 5, using different overlaps between the neighboring rings while keeping other conditions, e.g., the ion energy, the ion beam current, the processing time, and the milling mode, identical for (a) and (b). Thus, the ion dose is simply divided into three levels. But from the corresponding SEM side-view images in Figs. 5(a) and 5(b), it is clear that the milled structure was not simply of three height levels with regard to the applied pattern doses. The single-dosed areas were obviously etched slant as can be seen from the SEM side-view in Fig. 5(a), since the clear edge formed by the former ring pattern was milled by the following ring soon after. With ions scanning going on, the overlapping section is being milled into small slant and gradually stretched to the ring center. Finally, tower like structures were fabricated. With simply decreasing the outer diameter of the rings while keeping the inter distance unchanged, completely different cross-scale and hierarchical structures were obtained as shown in Fig. 5(b). Furthermore, by increasing the performing time, structures with higher aspect ratio can be obtained as shown in Fig. 5(c).

Beside the ion dose, the other very important factor that determines the shape and size of the resulted structures is the

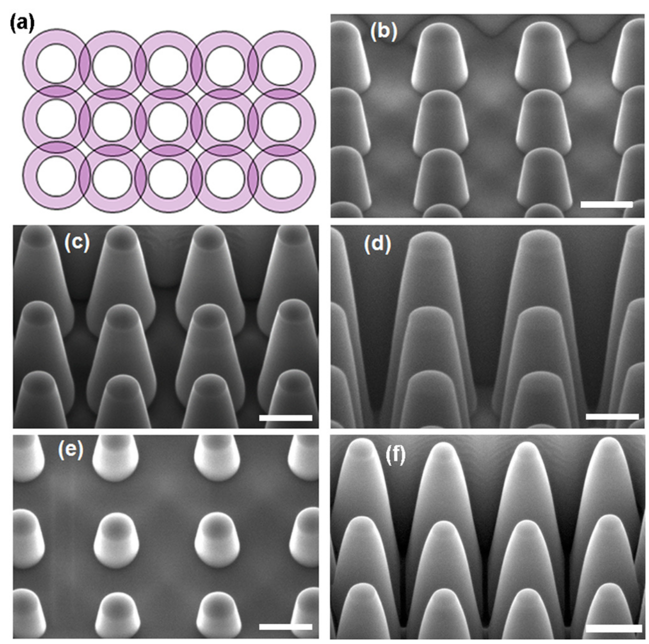

FIG. 6. The influence of the pattern size and overall ion-dose in FIB patterning of diamond with periodically-positioned-rings: (a) schematic arrangement of the pattern; (b)–(f) SEM side-view images of structures prepared with inner diameter of 600 nm for (c), 500 nm for (e) and 700 nm for (b), (d) and (f). The outer diameter was 1.2 μm. The scale bar is 2 μm.

inter-distance between the neighboring rings. For instance, when the pattern size reduced to sub-micrometer, the above discussed stray dose etching can be even more crucial and may act as the main factor that limits the feature size of a diamond nanostructure that can be produced. Fig. 6(a) shows the patterns used for such phenomena observation. As can be seen from the SEM side-view images in Figs. 6(b)–6(f) that areas enclosed by the four rings, where actually no ion dose was assigned, were also etched and almost being flattened with areas where single-dose was applied. Consequently, separated freestanding diamond structures were formed and uniformly distributed on the substrate surface. The effect of the etching time was also examined. Structures in Figs. 6(d) and 6(f) were milled using etching time consecutively doubled and tripled compared with that for (b). The effect of the pattern size was investigated by simply changing the inner diameter of the setting patterns. Figs. 6(b)–6(d) show the SEM side-view images that milled with various inner diameters. Clearly, by increasing the ion milling time, or by reducing the inner diameter, nanocones with thinner tip can be obtained. However, it should be noted that the top would be cut off if the inner diameter goes below some value (500 nm) under a certain ion beam current (2.5 nA), as shown in Fig. 6(e), a case in which stray-dose etching acted as an obstacle in achieving smaller nanostructures.

Again, NV^- centers were precisely positioned with a confocal optical microscope and 3D network structures were fabricated with single NV^- center embedded in nanopillar. Single photon property was characterized by the second order photon correlation function for the aimed NV^- center. Fig. 7(a) shows a typical SEM image of nanopillars, which could processed by FIB direct milling followed by dry and wet etching treatments for surface contamination removal, or alternatively, through electron-beam-lithography related techniques followed by reactive ion etching for patterning transfer. Fig. 7(b) is the second order intensity correlation function $g^{(2)}(\tau)$ of a pillar, which has a similar shape as indicated by the arrow in Fig. 7(b). It clearly suggests that the emission arises from a single center. The intensity of the bright spot in the fluorescence scanning image is about 480 kc/s for the nanopillar and single photons' count rate indicates an enhancement of about ten folds in the photon collection efficiency, compared with the un-sculptured diamond crystal,[22] and it is compared with that of the SIL previously reported in this work. However, for these structures, the current configuration is too compact for fabrication of coplanar waveguide. Different pattern distribution will be used to explore the free induction decay signal of the electron spin in a selected NV^- center before and after the fabrication process. Nevertheless, we have demonstrated that FIB over-lay patterning is an effective approach to produce 3D diamond hierarchy networks with enhanced single photon properties.

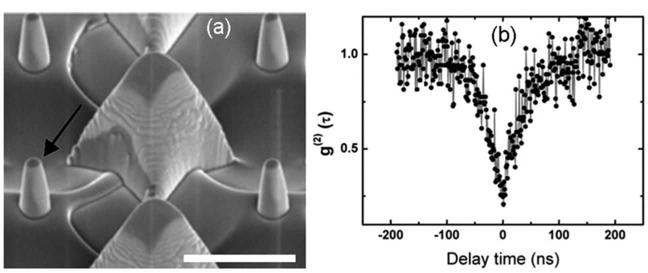

FIG. 7. (a) SEM image of diamond network structures and (b) second order photon correlation function of an NV^- center embedded nanopillar with a typical shape resembles that indicated by the arrow in (a).

IV. CONCLUSIONS

We developed an over-lay patterning method for fast, designable, and controllable fabrication of various 3D diamond micro-/nano-structures with FIB milling. SIL and nanopillar with NV^- center precisely placed at the designed location, which could enable efficient single-photon collection by overcoming the total internal reflection at the diamond/air interface, have been demonstrated. An enhancement of about ten folds of the single photons collection rate, well reserved long electron spin dephasing time, and single photon emission properties, has been obtained. Our results suggest that over-lay patterning could be an effective method to resolve the challenge in optical structure construction for employing diamond emitters in optical or quantum applications.

ACKNOWLEDGMENTS

This work is supported by the National Natural Science Foundation of China under Grants Nos. 91123004, 11104334, 51272278, 61390503, and 91023041, the 100 Technical Talent Program of the Chinese Academy of Sciences and the National Basic Research Program (973) of China under Grant No. 2014CB921400.

[1]C. A. Brookes, Nature **228**, 660 (1970).
[2]O. Faklaris, V. Joshi, T. Irinopoulou, P. Tauc, M. Sennour, H. Girard, C. Gesset, J.-C. Arnault, A. Thorel, J.-P. Boudou, P. A. Curmi, and F. Treussart, ACS Nano **3**, 3955 (2009).
[3]D. Luo, L. Wu, and J. Zhi, ACS Nano **3**, 2121 (2009).
[4]J. R. Maze, P. L. Stanwix, J. S. Hodges, S. Hong, J. M. Taylor, P. Cappellaro, L. Jiang, M. V. Dutt, E. Togan, A. S. Zibrov, A. Yacoby, R. L. Walsworth, and M. D. Lukin, Nature **455**, 644 (2008).
[5]L. Robledo, L. Childress, H. Bernien, B. Hensen, P. F. Alkemade, and R. Hanson, Nature **477**, 574 (2011).
[6]H. Bernien, L. Childress, L. Robledo, M. Markham, D. Twitchen, and R. Hanson, Phys. Rev. Lett. **108**, 043604 (2012).
[7]C. Kurtsiefer, S. Mayer, P. Zarda, and H. Weinfurter, Phys. Rev. Lett. **85**, 290 (2000).
[8]F. Jelezko, T. Gaebel, I. Popa, A. Gruber, and J. Wrachtrup, Phys. Rev. Lett. **92**, 076401 (2004).
[9]G. Balasubramanian, P. Neumann, D. Twitchen, M. Markham, R. Kolesov, N. Mizuochi, J. Isoya, J. Achard, J. Beck, J. Tissler *et al.*, Nature Mater.**8**, 383 (2009).
[10]A. Gruber, A. Dräbenstedt, C. Tietz, L. Fleury, J. Wrachtrup, and C. Borczyskowski, Science **276**, 2012 (1997).
[11]M. V. Dutt, L. Childress, L. Jiang, E. Togan, J. Maze, F. Jelezko, A. S. Zibrov, P. R. Hemmer, and M. D. Lukin, Science **316**, 1312 (2007).
[12]P. Neumann, J. Beck, M. Steiner, F. Rempp, H. Fedder, P. R. Hemmer, J. Wrachtrup, and F. Jelezko, Science **329**, 542 (2010).
[13]B. B. Buckley, G. D. Fuchs, L. C. Bassett, and D. D. Awschalom, Science **330**, 1212 (2010).
[14]L. Robledo, L. Childress, H. Bernien, B. Hensen, P. F. A. Alkemade, and R. Hanson, Nature **477**, 574 (2011).
[15]G. Balasubramanian, I. Y. Chan, R. Kolesov, M. Al-Hmoud, J. Tsisler, C. Shin, C. Kim, A. Wojcik, P. R. Hemmer, A. Krueger *et al.*, Nature **455**, 648 (2008).

[16]F. Dolde, H. Fedder, M. W. Doherty, T. Nöbauer, F. Rempp, G. Balasubramanian, T. Wolf, F. Reinhard, L. C. L. Hollenberg, F. Jelezko *et al*., Nat. Phys. **7**, 459 (2011).
[17]B. J. M. Hausmann, M. Khan, Y. Zhang, T. M. Babinec, K. Martinick, M. McCutcheon, P. R. Hemmer, and M. Lončar, Diamond Relat. Mater. **19**, 621 (2010).
[18]E.-S. Baik, Y.-J. baik, S. W. Lee, and D. Jeon, Thin Solid Films **377**, 295 (2000).
[19]Y. Tao and C. Degen, Adv. Mater. **25**, 3962 (2013).
[20]T. M. Babinec, B. J. Hausmann, M. Khan, Y. Zhang, J. R. Maze, P. R. Hemmer, and M. Loncar, Nat. Nanotechnol. **5**, 195 (2010).
[21]K.-M. C. Fu, C. Santori, P. E. Barclay, I. Aharonovich, S. Prawer, N. Meyer, A. M. Holm, and R. G. Beausoleil, Appl. Phys. Lett. **93**, 234107 (2008).
[22]T. M. Babinec, J. T. Choy, K. J. M. Smith, M. Khan, and M. Lončar, J. Vac. Sci. Technol. B **29**, 010601 (2011).
[23]S. Castelletto, J. P. Harrison, L. Marseglia, A. C. Stanley-Clarke, B. C. Gibson, B. A. Fairchild, J. P. Hadden, Y. L. D. Ho, M. P. Hiscocks, K. Ganesan, S. T. Huntington, F. Ladouceur, A. D. Greentree, S. Prawer, J. L. O'Brien, and J. G. Rarity, New J. Phys. **13**, 025020 (2011).
[24]D. M. Toyli, C. F. de las Casas, D. J. Christle, V. V. Dobrovitski, and D. D. Awschalom, Proc. Natl. Acad. Sci. **110**, 8417 (2013).
[25]J. P. Hadden, J. P. Harrison, A. C. Stanley-Clarke, L. Marseglia, Y. L. D. Ho, B. R. Patton, J. L. O'Brien, and J. G. Rarity, Appl. Phys. Lett. **97**, 241901 (2010).
[26]W. Hosler and W. Palmer, Surf. Interface Anal. **20**, 609 (1993).
[27]L. Childress, J. M. Taylor, A. S. Sørensen, and M. D. Lukin, Phys. Rev. Lett. **96**, 070504 (2006).
[28]M. A. Nielsen, Rep. Math. Phys. **57**, 147 (2006).
[29]L. Jiang, J. M. Taylor, A. S. Sørensen, and M. D. Lukin, Phys. Rev. A **76**, 062323 (2007).